Direct CFD Predictions of Low Frequency Sounds Generated by a Helicopter Main Rotor

Ben W. Sim
UARC/AFDD
Ames Research Center
Moffett Field, CA
ben.w.sim@us.army.mil

Mark A. Potsdam
U.S. Army AFDD
Ames Research Center
Moffett Field, CA
mark.potsdam@us.army.mil

Dave A. Conner
U.S. Army AFDD/JRPO
Langley Research Center
Hampton, VA
david.a.conner@nasa.gov

Michael E. Watts
Aeroacoustics Branch
NASA Langley Research Center
Hampton, VA
michael.e.watts@nasa.gov

ABSTRACT

The use of CFD to directly predict helicopter main rotor noise is shown to be quite promising as an alternative mean for low frequency source noise evaluation. Results using existing state-of-the-art grid structures and finite-difference schemes demonstrated that small perturbation pressures, associated with acoustics radiation, can be extracted with some degree of fidelity. Accuracy of the predictions are demonstrated via comparing to predictions from conventional acoustic analogy-based models, and with measurements obtained from wind tunnel and flight tests for the MD-902 helicopter at several operating conditions. Findings show that the direct CFD approach is quite successfully in yielding low frequency results due to thickness and steady loading noise mechanisms. Mid-to-high frequency contents, due to blade-vortex interactions, are not predicted due to CFD modeling and grid constraints.

NOTATION

α	Shaft tilt (corrected) or tip-path-plane angle
BPF	Blade passing frequency
C_T/σ	Thrust coefficient to rotor solidity ratio
M_{adv}	Advancing tip Mach number
μ	Advance ratio
Θ_0	Collective pitch angle, deg.
Θ_{ls}	Longitudinal cyclic pitch angle, deg.
Θ_{lc}	Lateral cyclic pitch angle, deg.
LFSPL	Low frequency sound metric (1st-6th BPF), dB
MFSPL	Mid frequency sound metric (> $6t^h$ BPF), dB
OASPL	Overall sound metric (Full-bandwidth), dB

INTRODUCTION

Computational Fluid Dynamics (CFD) methods have demonstrated ample fidelity and precision in simulating the aeromechanics characteristics of helicopter rotors. Many on-going efforts[1-4] have shown that, when coupled to Comprehensive Structural Dynamics (CSD) codes, the combined state-of-the-art CSD/CFD approach is capable of simulating realistic rotor trim solutions, performance, blade structural loads and blade airloads. Much of this success is attributed to CFD's abilities in capturing volumetric flow details surrounding the rotor, such as effects due to the rotor wake, and those due to three-dimensional, unsteady transonic flows over blade surfaces.

In recent years, these CSD/CFD prediction codes have shown even greater improvements with the advent of faster and more powerful computing platforms. Better correlations of predictions to experiment are foremost attributed to an increase in number of grid points used in the computational domain - to the extent that complex rotor aerodynamics and flow details at smaller length scales of interests can now be resolved. In conjunction with efforts tasked to develop new, higher-order finite difference schemes that minimize numerical errors, these coupled-CSD/CFD methods are promising to be a powerful and useful tool for accurate numerical studies and, eventually, for designing future rotorcraft.

Success in predicting near body aerodynamics of helicopter rotors naturally leads to the question if realistic acoustics pressure perturbations from the rotor can be captured by CFD as well. General consensus[5-7] dismiss the use of direct CFD numerical simulation for long range external acoustics radiation due to the small acoustics perturbations often obscured by accruing numerical dissipation/dispersion errors resulting from the implementation of finite difference schemes. Parasitic waves associated with wave reflections from ill-defined boundary flow conditions may also distort results. In many cases, these errors can be of the same order of magnitude, or even greater, compared to the acoustics pressure perturbations themselves where solutions are required at great distances from the source. The computations are also prohibitively expensive and time-consuming due to the vast number of grid points necessary to cover the spatial extent and the acoustics bandwidth of the problem.

These short-comings are less pronounced for characterizing source noise properties close to the source. Stronger acoustic signals (at closer proximity to the source) tends to yield better "signal-to-noise ratio" - suggesting that it may be possible to yield realistic acoustic pressures directly from CFD. The challenges lie in satisfying the inherently large spectral bandwidth requirement and also addressing the large disparity between acoustic pressure perturbations and mean flow pressures. For plausible CFD

---

implementations, this stipulates a grid spacing constraint that must be sufficiently small to represent the smallest wavelength (i.e. highest frequency) of interest associated with the source noise mechanism. Naturally, smaller grid spacing and large spatial domains of interest (related to observer locations) result in larger number of grid points that render direct CFD methods to be sometimes impractical.

While there are some modeling constraints with this approach, use of direct CFD method has been successfully demonstrated before by Baeder[8] in 1991. Euler-based CFD simulations were then performed for a non-lifting, hovering rotor at high tip Mach numbers known to produce strong High Speed Impulsive (HSI) noise due to delocalized weak shocks. Results illustrated the need to cluster grid points along known directions of sound propagation to yield satisfactory acoustics predictions that are in agreement with measurements up to two radii away from the rotor hub. Grid sensitivity studies also indicated the need for about 60,000 grid points to adequately capture the nonlinearities associated with the delocalized shock front. This effort clearly showed that acoustic predictions using CFD is possible if the grids are adequately structured and sufficient computational resources are available. The study, however, did not extend to realistic flight conditions with a lifting rotor operating at forward flight velocities and tip Mach numbers representative of typical helicopter flight envelope.

As an extension to the effort by Baeder, this paper will examine the ability of using CFD to directly predict radiating acoustic pressure waves from a helicopter main rotor (source noise) under more realistic circumstances. Emphasis will be placed on noise predictions near in-plane of the rotor that are of concern for military operations. Fidelity of the predictions will be evaluated via comparing results obtained from direct CFD methods to conventional acoustics analogy-based methods for a MD-902 main rotor. Measured acoustics data from wind tunnel and full-scale flight testing will also be used when possible. With such a wide range of source noise prediction models and source noise measurements for comparisons, it is the goal of this paper to:

• Determine the feasibility of direct CFD methods in capturing the source noise of a helicopter main rotor in steady-state forward flight lifting conditions. Note that the cases in this paper are limited to Mach numbers below delocalization, such that both the acoustic thickness and loading components are significant in the sound generation mechanism.

• Highlight the state-of-the-art using existing CFD algorithms and grid structures, deemed appropriate for accurate rotor aerodynamics modeling, directly for acoustics predictions. Grid clustering efforts, though known to generate better results, are not a focus of this study.

SOURCE NOISE PREDICTIONS

The ensuing section provides a description of the different source noise prediction methodologies used in the paper. In particular, the procedures to extract acoustic pressures directly from CFD results are highlighted and compared to conventional acoustic analogy-based methodologies. The pros-and-cons of each approach are also discussed.

Direct CFD Acoustics Predictions (DCAP)

CFD calculations use the complex geometry Navier-Stokes solver OVERFLOW 2.1ad[9]. Capabilities for loose (delta) coupling have been added to the NASA release version based on original developments under the DoD CHSSI Portfolio, Collaborative Simulation and Testing (CST-05)[10]. OVERFLOW computes solutions on structured, overset grids using a near- and off-body discretization paradigm (Fig. 1). The near-body grids surround the solid surfaces and capture the viscous effects with highly stretched curvilinear meshes. They extend out approximately one chord from the rotor blade. Automatically generated Cartesian off-body grids surround the near-body grids and capture the wake. They extend out to the far field boundary, placed at 5 rotor radii, with increasing spacing. There is a factor of 2 spacing between successive off-body grid levels. Time-accurate simulations of complex aircraft configurations with aeroelastic bodies in relative motion can be efficiently computed on parallel processors using the overset methodology.

The computational structural dynamics (CSD) calculations use the CAMRAD II v4.6 (Johnson) comprehensive rotorcraft analysis software, based on the baseline DARPA Helicopter Quieting Program MDART/SMART model input. The dual load path root (pitchcase and flexbeam) and blade are modeled with 10 elements, along with a compliant pitch link. The flexbeam has one axial degree-of-freedom. A harmonic analysis is performed using 18 blade modes. CAMRAD II performs both the CSD and rotor trim. Details of the structural modeling are provided in Potsdam2.

CFD/CSD coupling between OVERFLOW and CAMRADII is performed using a conventional (for rotorcraft) loose coupling incremental "delta" formulation[1]. Coupling is on a per revolution basis based on periodicity. Motions (3 rotations and 3 translations of the airfoil sections) and airloads (section normal force, chord force, and pitching moment) are exchanged. Fully-automated coupling is performed using shell scripting, file I/O, and interface programs. Typically, 7 coupling iterations are used, with 2/5 rev (2 blade passages for the 5-bladed rotor) between each coupling.

The MD-902 main rotor is comprised of 5 blades and a high fidelity hub. Each blade is composed of 3 grids (root cap, blade, tip cap). Excluding tip caps, the main portions of

the blade are O-grid topology. The chordwise, spanwise, and normal dimensions are 221 x 248 x 59 for the main blade, with 21 points across the blunt trailing edge. The baseline grid contains 56.1 million points (67% off-body) in 62 grids. The finest Cartesian off-body level 1 (L1) grid has 8% mean chord wake spacing. It surrounds the rotor and captures the wake with dimensions ±1.1R in X and Y, and –0.14R, +0.20R in Z. There are 3.4 million points per blade. Solutions were run on 256 processors at 10.4 hours per rotor revolution on a Cray XT5.
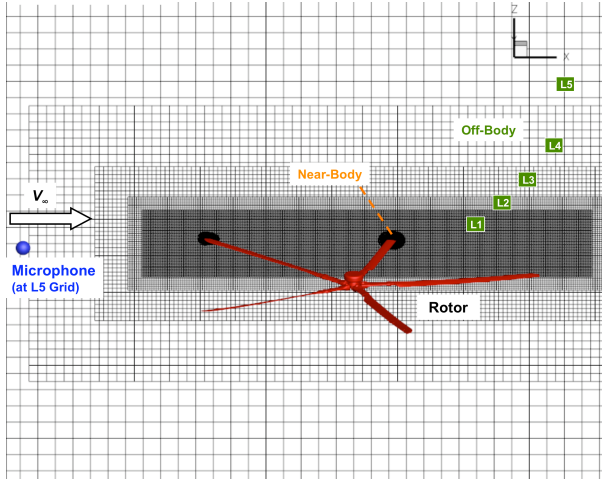
Figure 1. Baseline CFD over-set grid.

The time-accurate calculations use a high order 6th-order central difference spatial discretization with added 6th-order scalar (near-body) and matrix (off-body) artificial dissipation, resulting in a nominally 5th-order scheme[12]. A 7-point stencil is required, and the overset Cartesian meshes have triple fringing. A 2nd-order temporal backward difference scheme with iterative dual time stepping is used for time advancement along with a penta-diagonal left-hand side scheme. Fifteen (15) sub-iterations are used, typically resulting in 1.5 – 2.0 orders of magnitude reduction in the main blade grid residuals and considerably more (> 3.0) in the off-body grids. Quarter degree (0.25°) time steps are used (1440 steps per rotor revolution). The Spalart-Allmaras turbulence model is employed in the near-body grids. The off-body wake grids are inviscid.

Solutions are run from scratch for 3 rotor revolutions using previously computed CFD/CSD coupled motions. The last revolution is recorded for acoustics analysis. The flow field data is saved at 1-degree intervals. Saving the complete flow solution this frequently is very slow and inefficient. It generates a huge amount of data which must then be manually manipulated and stored. Instead, it is much more efficient to record the minimal amount of data needed. To this end the $SPLITM capability in OVERFLOW 2.1ad has been used. Data is stored on a Y plane at the microphone location (y = 0.63R) extracted from the off-body grids only. The pressure at the nearest point to the microphone in this 2D data subset is then extracted in a simple post-processing

step to generate the pressure signal. In-plane data (z = 0) from the off-body meshes is saved for visualization purposes. Finally, surface data from the near-body grids is saved for on-surface non-compact noise predictions using WOPWOP. The grid and flow solution files for these three 2D datasets (y = .63R, z = 0, and solid surfaces) require 66 MB per time step, compared with 8.8 GB for the entire flow field. They represent less than 1% of the flow field data. Similarly, acoustic data surfaces, such as Pringles or tuna cans (Bain), for permeable surface FW-H analysis can be saved efficiently using the $ADSNML capability, which interpolates flow field data onto arbitrary user specified 2D grids. A severe limitation with ADS surfaces in OVERFLOW requires that these grids reside within the L1 domain. At this time, this generally precludes extracting hemisphere maps or ground plane acoustics data directly.

Other limitations include a bandwidth restriction on the acoustics data that is inherently governed by the grid spacing at the point of evaluation. The relatively coarse spacing (Fig. 1), away from the rotor, suggests it is unlikely that mid-to-high frequency contents, such as those due to blade-vortex interactions or high-speed impulsive noise, can be captured without grid refinement. The general rule-of-thumb is to approximate this upper frequency limit using at least five grid points per wavelength. For full-scale rotor studies, an off-body grid spacing on the order of 12 inches would yield a cut-off frequency of about 200 Hz – thus, preventing higher frequencies to be captured. It is also noted that this approach, unlike acoustic analogy-based methodologies, does not allow contributions from thickness and loading noise components to be evaluated separately.

Nonetheless, the direct extraction from CFD results is deemed an attractive solution as it eliminates the need for a separate acoustics analysis in the computational chain. It is also deemed favorable for accounting any flow-field effects (quadrupole contributions off the blades) that may contain strong non-linearities caused by compressibility and flow separations.

Acoustic Analogy, On-Surface (FWH)

For comparison purposes, PSU-WOPWOP[13] is used to generate acoustics predictions based on the classical acoustic analogy approach, first proposed by Lighthill, and subsequently adapted by Ffowcs-Williams/Hawkings and Farassat for moving bodies. This approach is typically executed at the end of the computational chain after blade geometry, blade motion and aerodynamic load information have been resolved. In this paper, blade geometry and CFD-predicted blade surface pressures (non-compact) are supplied to PSU-WOPWOP to enable "on-surface" acoustics predictions in the time domain – accounting for only the linear thickness noise source and "on-surface" loading noise source terms. Volumetric data, associated with "off-surface" flow-field features important for the nonlinear quadrupole source term, are not considered in this paper.

SOURCE NOISE MEASUREMENTS

Acoustic measurements will also be used in this paper to evaluate the fidelity of DCAP noise predictions. The bulk of which is obtained from the Boeing-SMART rotor test, completed in 2008. Selective test points from a full-scale MD-902 acoustics flight test conducted in 2007 are also used in subsequent discussions.

Boeing-SMART Rotor Test (WT)

This paper relies on results obtained from the joint DARPA/NASA/Army-funded program[17] utilizing the Boeing's Smart Material Actuated Rotor Technology (SMART) rotor, tested in the 40- by 80-Foot Wind Tunnel of the National Full- Scale Aerodynamic Complex (NFAC) at NASA Ames Research Center in 2008 (Fig. 2a), as a guide for prediction validation. The Boeing-SMART rotor is a 34-ft diameter, full-scale, bearingless, five-bladed main rotor modified from an existing MD-902 Explorer rotor system with active trailing-edge flaps. An array of microphones was strategically placed around the full-scale model to capture rotor noise. The general layout of microphone placement in the wind tunnel is illustrated in Figure 2b – with details of their location coordinates listed in Table 1. For present study, this paper will primarily focus on in-plane microphone M13 and on selective test conditions with the active trailing-edge flaps un-deployed. All results were obtained with the rotor trimmed to a target thrust and minimized flapping moments.

a) SMART Rotor Testing in NFAC
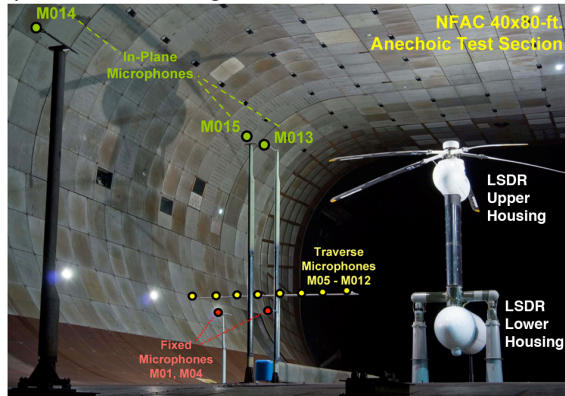
b) Microphone Layout (Top View)
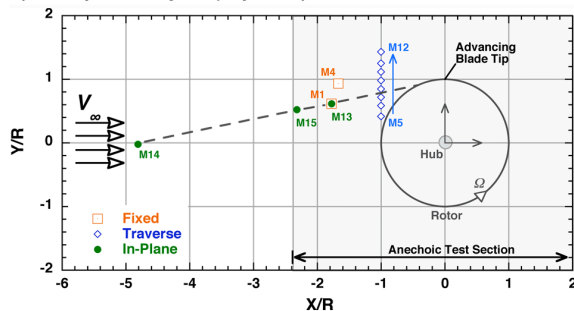
Figure 2. Boeing-SMART rotor: a) installation in wind tunnel, b) microphone layout.

Table 1. Microphone positions

Sensor Name	Cartesian[1]			Notes
	X, ft	Y, ft	Z, ft	
M01	-29.67	10.27	-17.94	Fixed Microphones
M04	-27.92	15.59	-17.87	
M05	-16.73	6.97	-15.13	Traverse Microphones (station: −200)
M06	-16.73	9.79	-15.13	
M07	-16.73	12.02	-15.13	
M08	-16.73	14.17	-15.13	
M09	-16.73	16.42	-15.13	
M10	-16.73	18.67	-15.13	
M11	-16.73	20.90	-15.13	
M12	-16.73	23.92	-15.13	
M13	**-29.67**	**10.27**	**-5.34**	**In-Plane Microphones**
M15	-38.77	8.73	-7.13	
M14	-80.36	-0.33	-14.84	

Note[1] hub-centered, 0 deg. shaft tilt
X – positive towards aft of rotor, Y – positive towards starboard, Z – positive up

Acoustics data were acquired for 64 revolutions, at a rate of 2048 samples per revolution. The time records are subsequently averaged, on a per-rev basis, to isolate harmonic contents pertaining only to the rotation of the rotor. As reported in Ref. 18, these measurements contain reflections due to the presence of non-ideally treated wind tunnel walls. Also, it should be noted that these acoustic data were acquired in a configuration where the rotor and microphone were fixed at the same relative distance - similar to the setup in the prediction methodologies described above.

Eglin III Acoustics Flight Test (FT)

Acoustics data were also extracted from a MD-902 helicopter flight test[19], conducted at Eglin Air Force Base in 2007, for comparisons in this paper. The NOTAR-platform provides an excellent source of data for comparisons to main rotor-only wind tunnel test data and predictions. As described in Ref. 19, the flight test program utilized 19 ground-fixed microphones in a horseshoe-shaped array to create source noise hemispheres for various level and descent flight profiles. An extensive array of instrumentations, including a Differential Global Positioning System (DGPS) unit, a real-time pilot guidance and a tethered-weather balloon system, were used to monitor the vehicle's flight track, performance state and atmospheric conditions.

To enable direct comparisons with the afore-mentioned wind tunnel/prediction data, segments of the measured flight test time history data (approximately five revolutions long) were extracted from a selected ground-fixed microphone that geometrically simulates the source-to-microphone directivity (emission angles[1]) of the wind tunnel microphone M13 shown in Figure 2b. The data are subsequently de-

---

[1] Emissions angles were calculated using the advancing blade tip as the origin.

dopplarized to be consistent with measurements obtained in the non-stationary medium inherent in both wind tunnel measurements and predictions. In addition, the amplitudes are adjusted using the 1/r-spherical spreading rule to match source-to-microphone distance for wind tunnel microphone M13 and also re-conditioned to remove ground reflection effects. Results are subsequently cycle-averaged (using five revolutions of data) to generate a representative acoustic time history of the main rotor source noise over one rotor revolution.

CASE STUDY: MDART

The ensuing section makes use of a well-studied test condition from the Boeing-SMART Rotor wind tunnel test, known as MDART, for initial study. The MDART condition simulates the MD-902 main rotor operating at a level flight of 124 knots ($\mu = 0.30$). (See Table 2 for details of the rotor operating conditions.) All acoustics calculations are based on microphone M13 in the wind tunnel.

Figure 3 illustrates a snapshot (top view) of the perturbation pressure contours in the rotor plane predicted by DCAP obtained at an instant when microphone M13 sees the arrival of a strong acoustic wave-front. Contour levels are described in decibels (dB) using the absolute instantaneous perturbation pressures referenced to 2 x 10^{-5} Pascals. Predictions were made with the microphone located in the L5 off-body grid that has a grid spacing of approximately one blade chord. These results show that DCAP can, not only capture the pressure fluctuations associated with the vortex-wake system and downwash near the rotor, but also pressure waves from the advancing side of the rotor that radiates forward. The latter essentially constitute the acoustics waves that propagate into the far-field.

Figure 4 illustrates the acoustic time histories over one rotor revolution for the MDART case at microphone M13. Results from direct CFD predictions (DCAP) and from PSU-WOPWOP (FWH) are compared against measurements obtained from the Boeing-SMART wind tunnel test (WT) and from the Eglin III acoustics flight test (FT). All of these acoustic time histories show five dominant peak negative pressure pulses per rotor revolution. Each of the negative pulse is attributed primarily to the thickness noise originating from each of the five blades on the MD-902 main rotor system. No impulsive blade-vortex interactions-liked noise fluctuations are evident at this test condition.

Figure 5a shows a zoomed-in view of one of the peak negative pressure pulse. The Direct CFD method (DCAP) demonstrates that it is capable of capturing general features associated with the negative peak pressure pulse, albeit under-predicting the negative peak amplitude when compared to measurements. In comparison, predictions

from the on-surface acoustic analogy method (FWH) is worse, with only half of the negative peak accounted for. Although not shown in this paper, this discrepancy is likely caused by the negligence of flow-field/compressibility effects off the tip of the rotor blade observed in Figure 3. Off-surface FWH implementations will likely facilitate better predictions.

Similar trends are observed with acoustic time histories lowpass-filtered at 200 Hz (Fig. 5b). As discussed previously, this cut-off frequency is associated with DCAP's bandwidth limitations using a grid spacing of 12.8 inches (approximately one blade chord) at microphone M13. In the frequency domain (Fig. 5c), this translates to the ability to account for only the harmonic contents at and below the 6th blade passing frequency (BPF) harmonic for the MD-902 rotor. Compared to wind tunnel results, predictions from DCAP in Figure 5c show much larger discrepancies at and beyond the 6th BPF harmonic. Low frequencies, below 6th BPF harmonic, are better predicted (to within 2 dB), with the exception of the 3rd BPF harmonic.

Also of interest to note is that while flight test time histories correlate quite well with wind tunnel measurement, there is a significant first BPF harmonic contribution in the flight test measurement not observed else where. In addition, it is unclear why the pulse width obtained from flight test is larger than those obtained in the wind tunnel. It is also indicated in the time histories that the wind tunnel data contains some spurious fluctuations not present in the flight test/predictions. These fluctuations have been determined to be due to wind tunnel wall reflections.

SENSITIVITY STUDIES

The MDART test condition is also used to examine effects of different CFD implementations to demonstrate their ability to capture small amplitude acoustic pressure waves.

Grid Spacings

Figure 6 shows the perturbation pressure contours for a case where the microphone M13 resides on a finer mesh. This is achieved in the CFD by extending the L1 grid forward to embody microphone M13. Doing so resulted in increasing the grid domain to 67.2 million total points and reducing the grid spacing at the microphone to about 0.8 inches (approximately one-tenth of the blade chord). Figure 6 shows that, although the refined grid results offered more details and smoother contours in the vicinity of the microphone, the overall patterns remain quite similar to the coarser grid solution shown in Figure 3.

Table 2. Rotor operating conditions for simulations and measurements

Parameters	Flight Conditions				Control Angles			Hub Forces			Hub Moments		
	μ	M_{adv}	α	C_T/σ	Θ_0	Θ_{1s}	Θ_{1c}	Lift	Drag	Side	Pitch	Roll	Torque
Units			deg.		deg.	deg.	deg.	lbf	lbf	lbf	in-lbf	in-lbf	in-lbf
WT[1]	0.300	0.806	-9.1	0.0804	10.60	6.13	-1.64	6003	-64	-139	11551	6356	110094
FT[2]	0.294	0.785	-8.6	0.0795	--	--	--	--	--	--	--	--	--
DCAP[3]	0.300	0.806	-9.1	0.0804	9.73	6.31	-2.11	5988	67	-122	558	1044	108757
FWH[4]	Same as DCAP												

Notes:
1   Measured, Boeing-SMART Rotor test (FY 2008), Run 46, Point 94
2   Measured, Eglin III Acoustics Flight test (FY 2007), Flight 102-273
3   CAMRADII/OVERFLOW-2 calculations trimmed to measured wind tunnel conditions and rotor thrust (min. hub moments)
4   Make use of OVERFLOW-2 predicted surface pressures at the same trim conditions as in DCAP
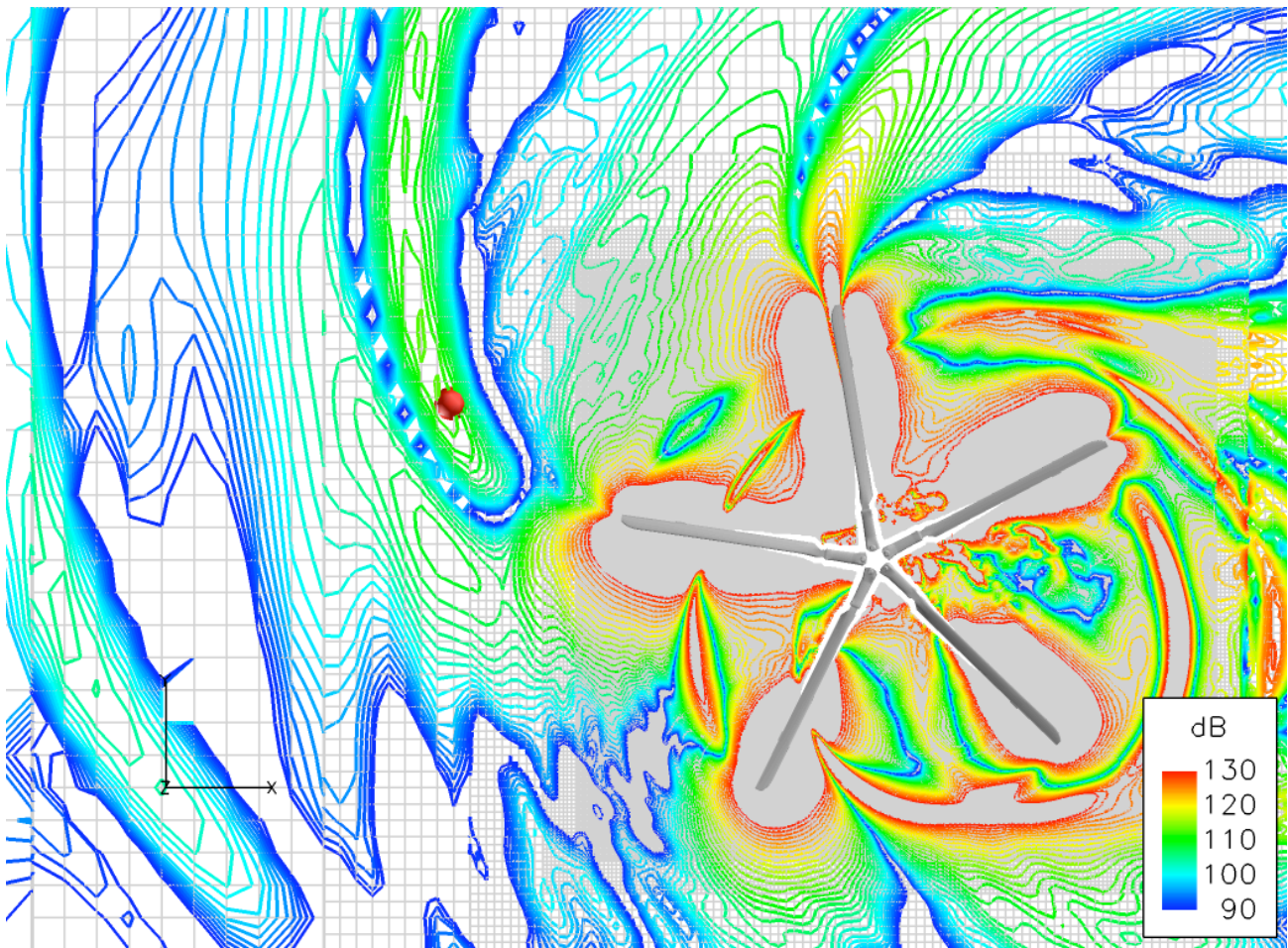
Figure 3. DCAP-predicted perturbation pressure contours for MDART case.
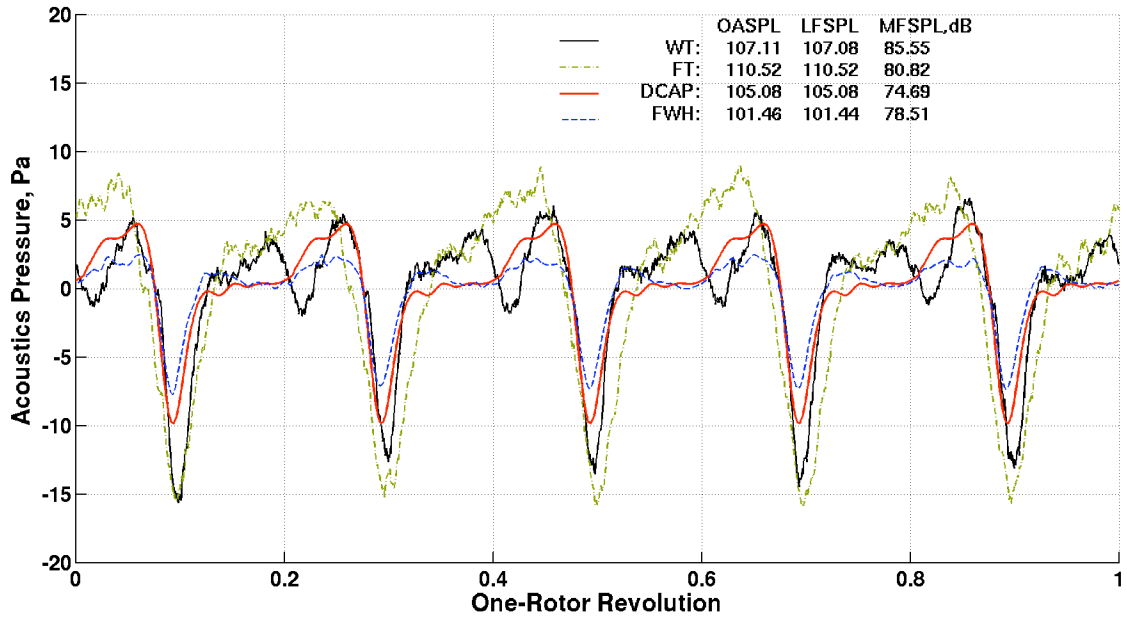
Figure 4. Predicted acoustic time histories for MDART case at microphone M13.
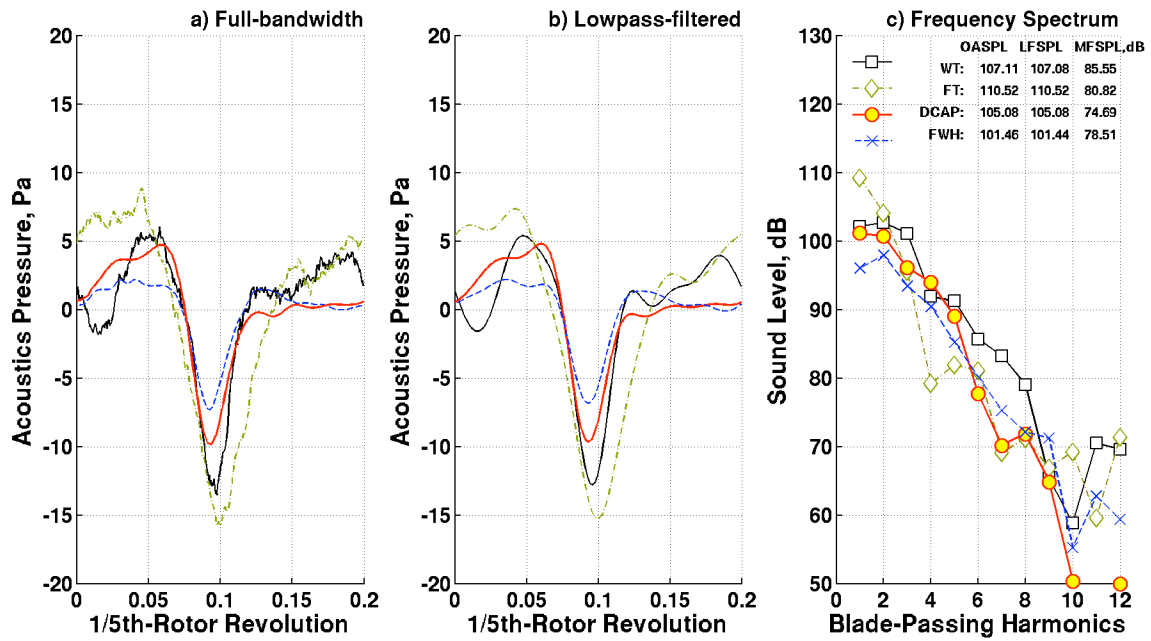

Figure 5. MDART case study: a) full-bandwidth time history, b) lowpass-filtered time history, c) frequency spectrum.

The effects on acoustics time histories are illustrated in Figure 7. Using the finer mesh (DCAP-L1) resulted in a slightly larger negative peak pressure compared to solutions obtained from the coarser grid (DCAP-L5). Overall, the effect seems to enhance the fidelity of direct CFD-based predictions to better correlate with wind tunnel measurement. Because of smaller grid spacing, the finer mesh solution is also able to capture sound levels at higher frequencies.

Finite-Difference Scheme

Results are also shown using a 3rd order scheme in the CFD model, as compared to the 5th order scheme discussed previously (Fig. 8a). Surprisingly, solutions obtained from the lower order scheme (DCAP-3rd) show comparable predicted peak negative pressure as from the 5th order scheme (DCAP-5th). Some differences, off to the side of the negative pressure peak, are observed between the two solutions, but are not significant enough for considerations. The primary difference lies in the predicted frequency spectrum (Fig. 8c) where the lower order scheme is shown to be unable to capture the higher frequency content of the acoustics radiation.
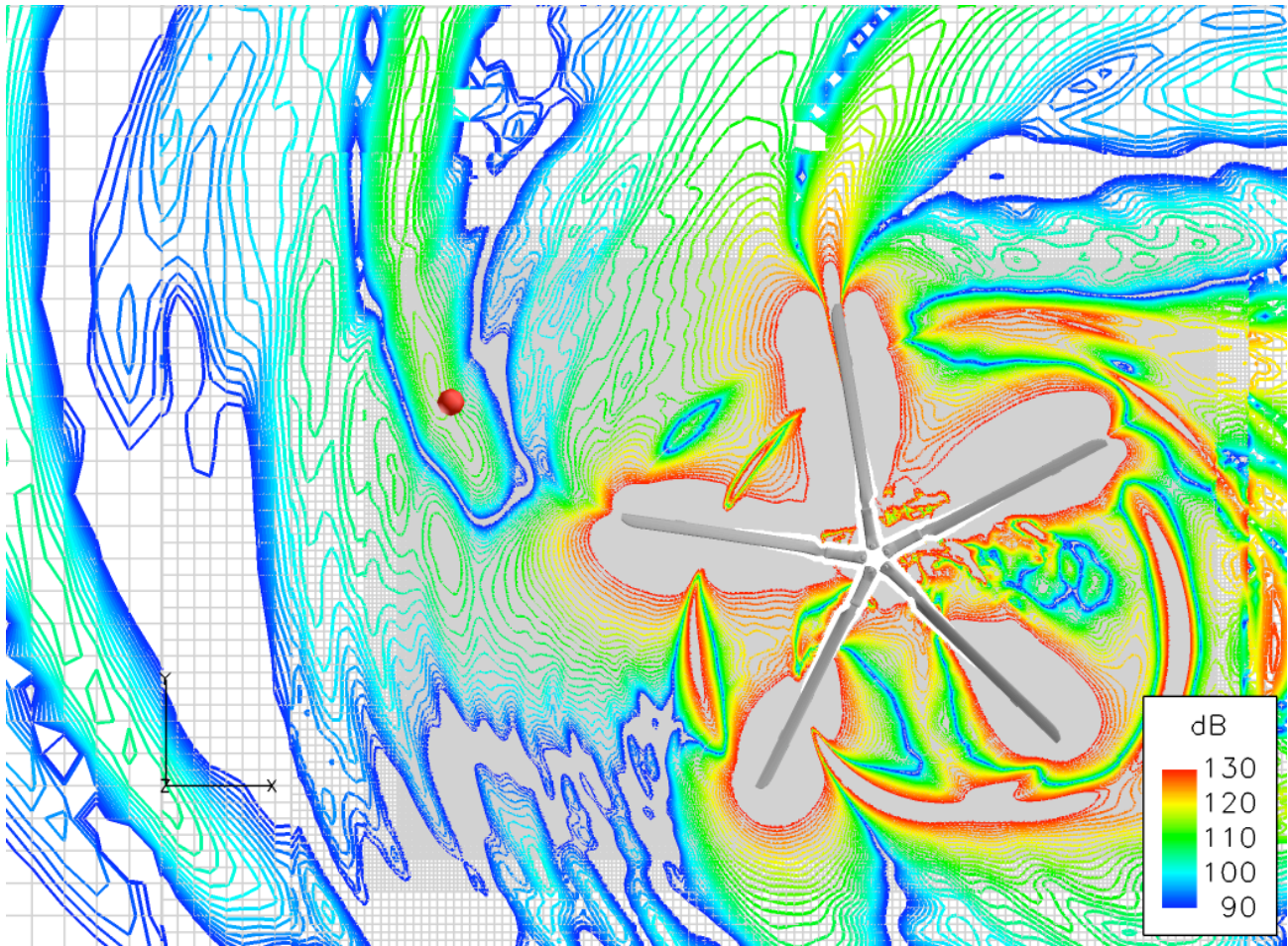

**Figure 6. DCAP-predicted perturbation pressure contours with finer mesh.**
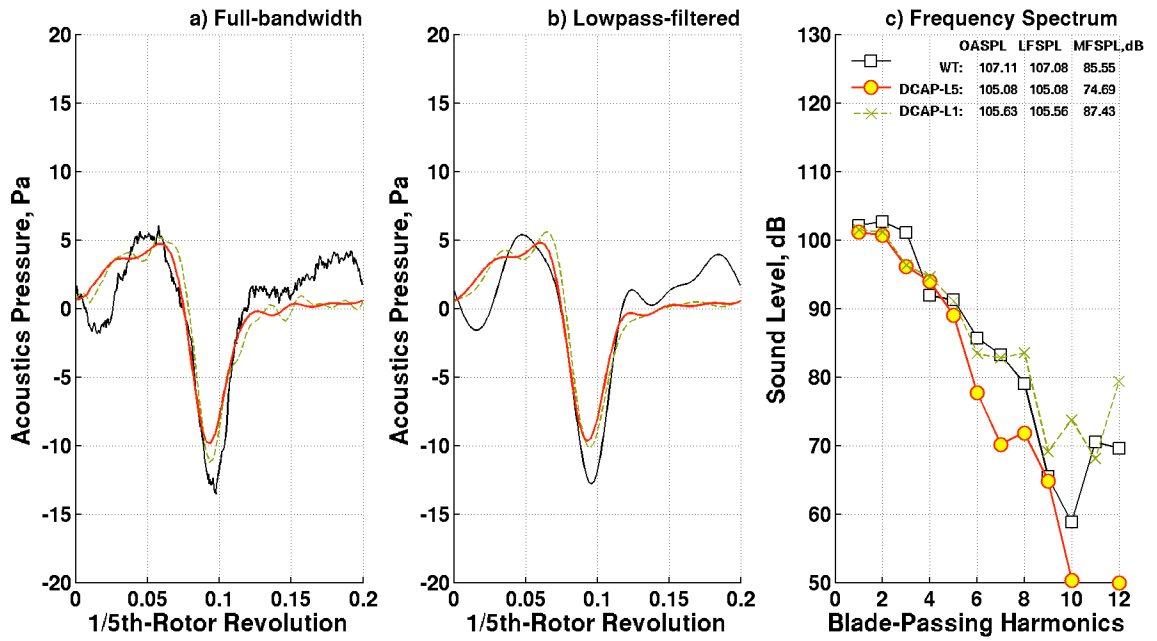
Figure 7. Grid dependence study: a) full-bandwidth time history, b) lowpass-filtered time history, c) frequency spectrum.
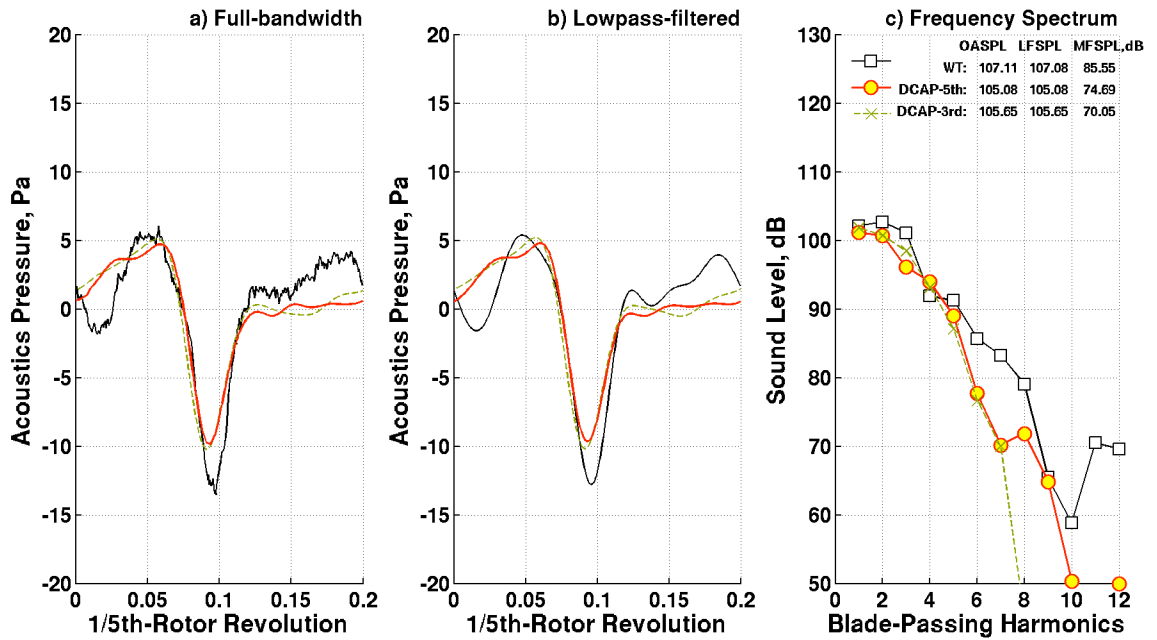

Figure 8. Finite-difference scheme sensitivity study: a) full-bandwidth time history, b) lowpass-filtered time history, c) frequency spectrum.

ADVANCE RATIO VARIATIONS

Robustness of the direct CFD method is highlighted in this section via evaluating the fidelity of DCAP predictions at for four different advance ratio conditions (Table 3). DCAP predictions are compared to acoustic analogy-based predictions, as well as measurements from wind tunnel, and flight test. First two conditions at lower advance ratios (μ = 0.165 and 0.200) pertain to strong BVI noise conditions during descent. As shown in Figure 9, distinct blade-vortex interaction fluctuations are present in the predicted airloads (normal force and chord force) and pitching moment at 87% span location. The μ = 0.250 condition represents a shallower descent with less BVI-induced aerodynamics fluctuations. Finally, the μ = 0.300 condition simulates a level flight condition at close to 123 knots. In all these cases, the rotor thrust was held approximately the same at a nominal C_T/σ of approximately 0.075. All calculations are performed with the same overset grid (a grid spacing of 12.8 inches at microphone M13) and 5th order scheme.

Table 3. Rotor operating conditions for speed variation study.

Parameters		Flight Conditions				Control Angles			Hub Forces			Hub Moments		
	μ	M_{adv}	α	C_T/σ	Θ_0	Θ_{1s}	Θ_{1c}	Lift	Drag	Side	Pitch	Roll	Torque
Units			deg.		deg.	deg.	deg.	lbf	lbf	lbf	in-lbf	in-lbf	in-lbf
$\mu \approx 0.165$													
WT	0.164	0.721	2.7	0.0754	4.47	2.02	-2.29	5746	-221	-162	11232	1436	35353
DCAP	0.164	0.721	2.7	0.0754	3.89	2.11	-2.17	5737	60	-92	-961	1510	33778
FW-H			Same as DCAP										
$\mu \approx 0.200$													
WT	0.200	0.748	-2.6	0.0764	4.21	2.22	-1.94	5856	-159	-165	13493	3186	30220
DCAP	0.200	0.748	-2.6	0.0764	3.71	2.51	-1.97	5837	79	-91	-3194	1530	29477
FW-H			Same as DCAP										
$\mu \approx 0.250$													
WT	0.250	0.779	-3.6	0.0756	7.01	4.15	-1.56	5789	-106	-146	8595	4923	62819
DCAP	0.250	0.779	-3.6	0.0756	6.24	4.20	-1.90	5755	90	-99	2181	165	60266
FW-H			Same as DCAP										
$\mu \approx 0.300$													
WT	0.300	0.810	-8.8	0.0749	10.27	6.20	-1.68	5695	-91	-142	5483	2656	106449
FT	0.307	0.791	-9.3	0.0760	--	--	--	--	--	--	--	--	--
DCAP	0.300	0.810	-8.8	0.0749	9.29	6.05	-1.92	5745	78	-103	2315	1933	102171
FW-H			Same as DCAP										

1 CAMRADII/OVERFLOW-2 calculations trimmed to measured wind tunnel conditions and rotor thrust (min. hub moments)
2 Make use of OVERFLOW-2 surface pressures calculated at the same trim conditions as in DCAP
3 Measured, Boeing-SMART Rotor test (FY 2008), Run 46, Point 94
**4** Measured, Eglin III Acoustics Flight test (FY 2007), Flight 102-273
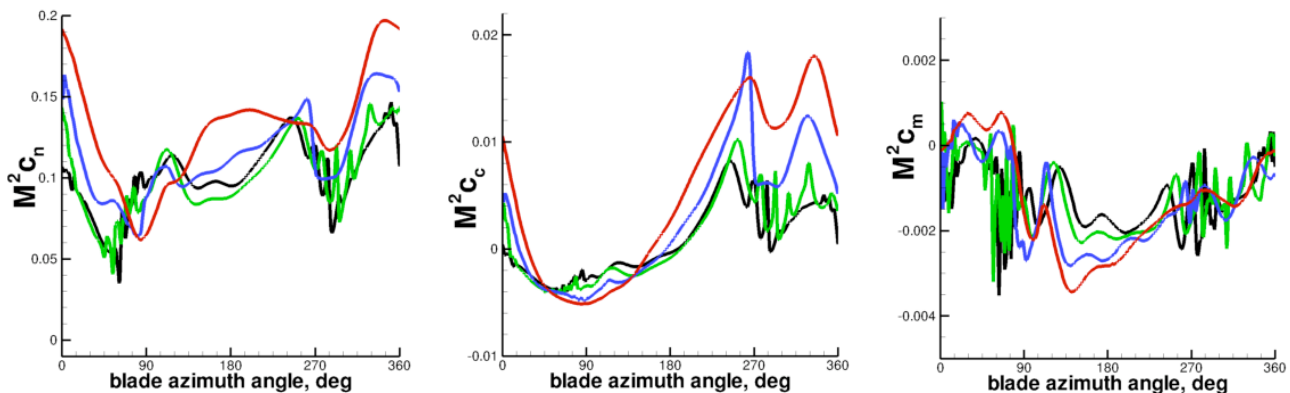
Figure 9. Predicted airloads and pitching moments at 87% span for the four different advance ratio conditions.

Figure 10 illustrates the CFD predicted perturbation pressure contours in the plane of the rotor for the different advance ratio conditions. Acoustic pressure wave-fronts generated by each of the blade can be seen to radiate forward from the advancing side of the rotor. As these wave-fronts arrive at microphone M13, Figure 10 illustrates that the perturbation pressures increase in strength with increasing advance ratios. Much of this is attributed to increased compressibility effects when a blade approaches the advancing side of the rotor near 90 degrees azimuth. It is also illustrated in Figure 10 that the flow-field off the blade tip, near the advancing side of the rotor, tends to become more prominent at higher advance ratios. This suggests that an off-surface approach is likely required to completely model the rotor acoustics at higher advance ratios

a) $\mu = 0.165$
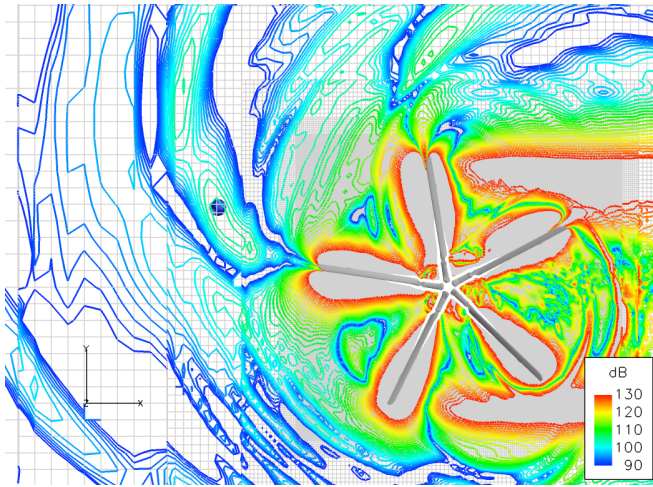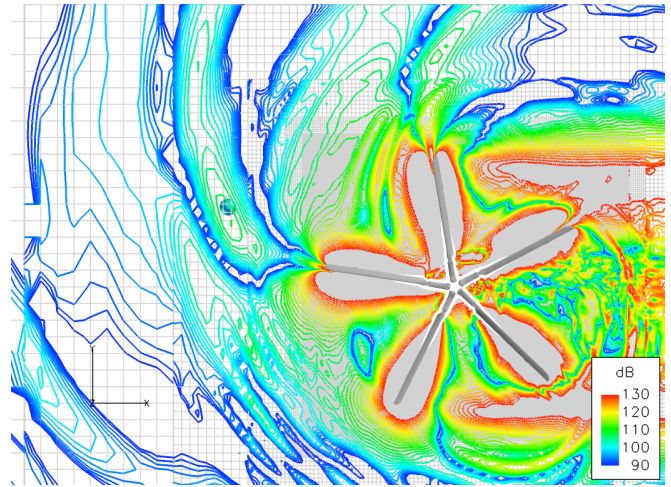
b) $\mu = 0.200$

c) $\mu = 0.250$
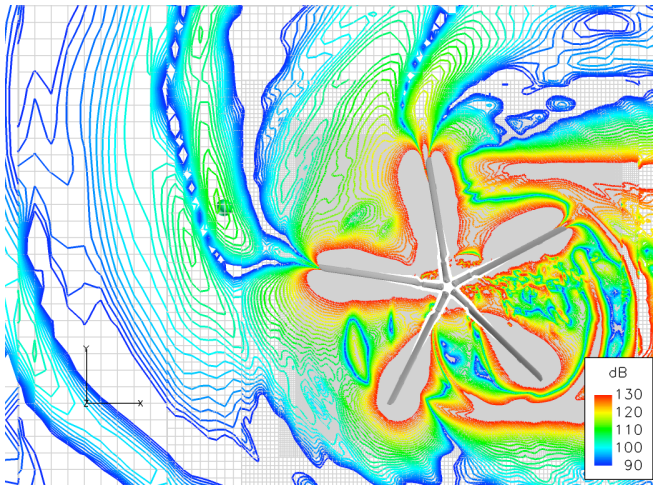
d) $\mu = 0.300$
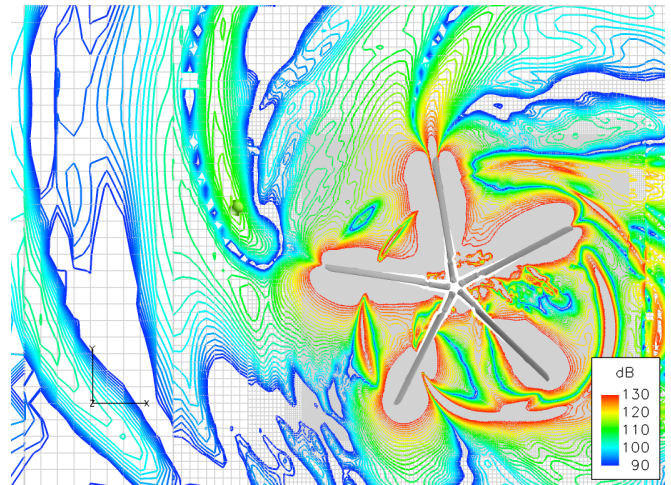
Figure 10. DCAP-predicted perturbation pressure contours at different advance ratios.

a) $\mu = 0.165$
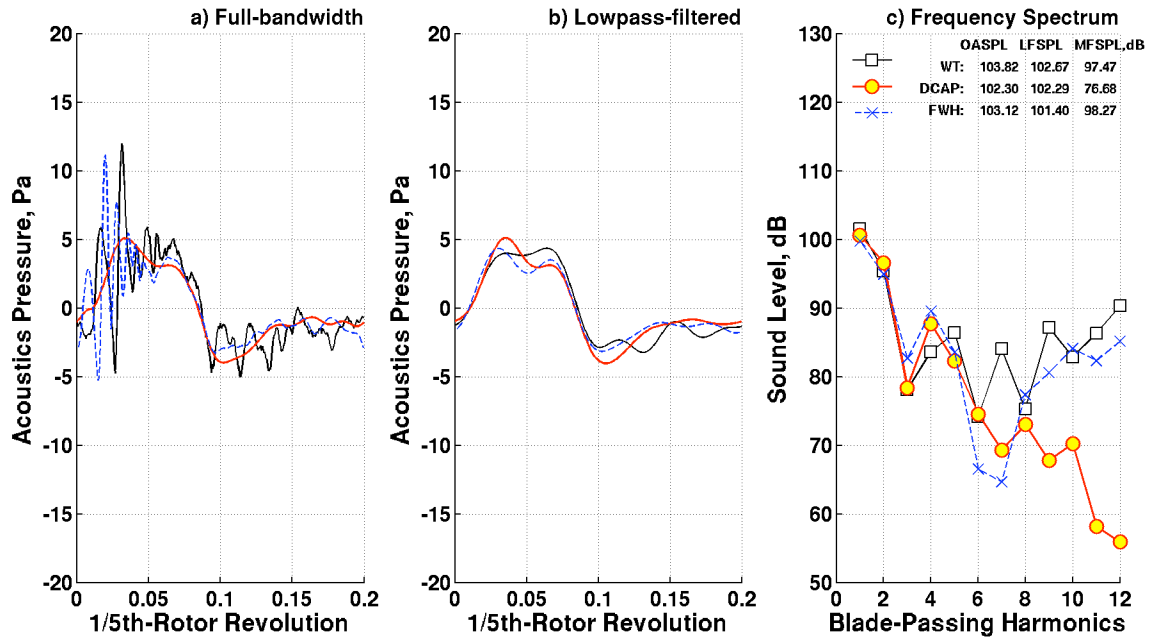
b) $\mu = 0.200$
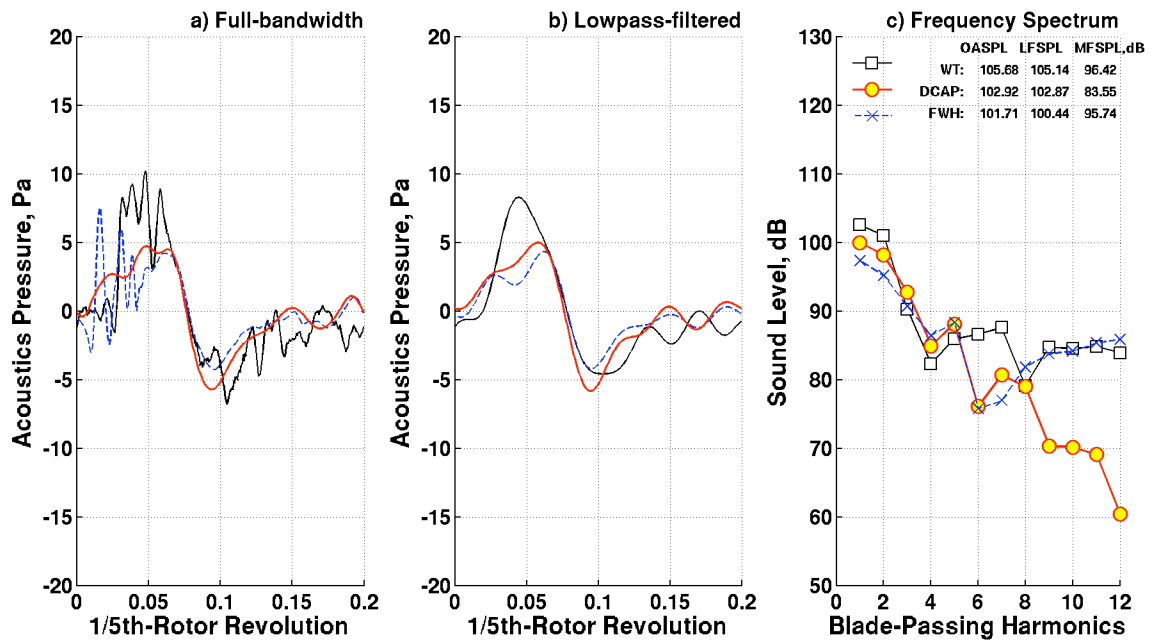
Figure 11. Predicted acoustic time histories for the different advance ratios at microphone M13.

c) $\mu = 0.250$
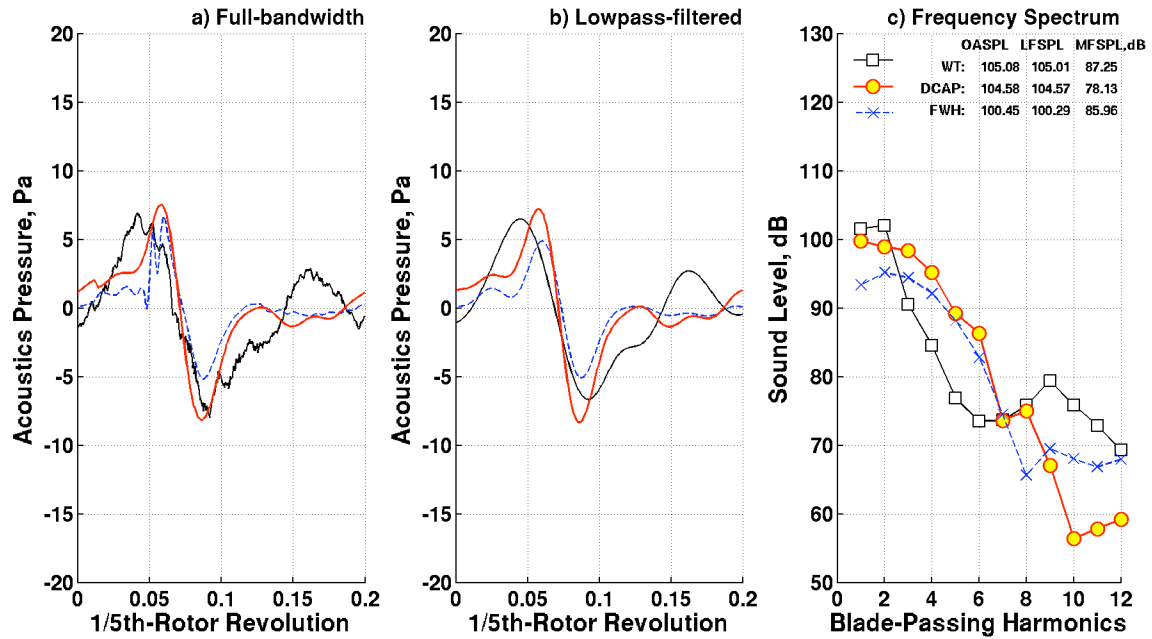
d) $\mu = 0.300$
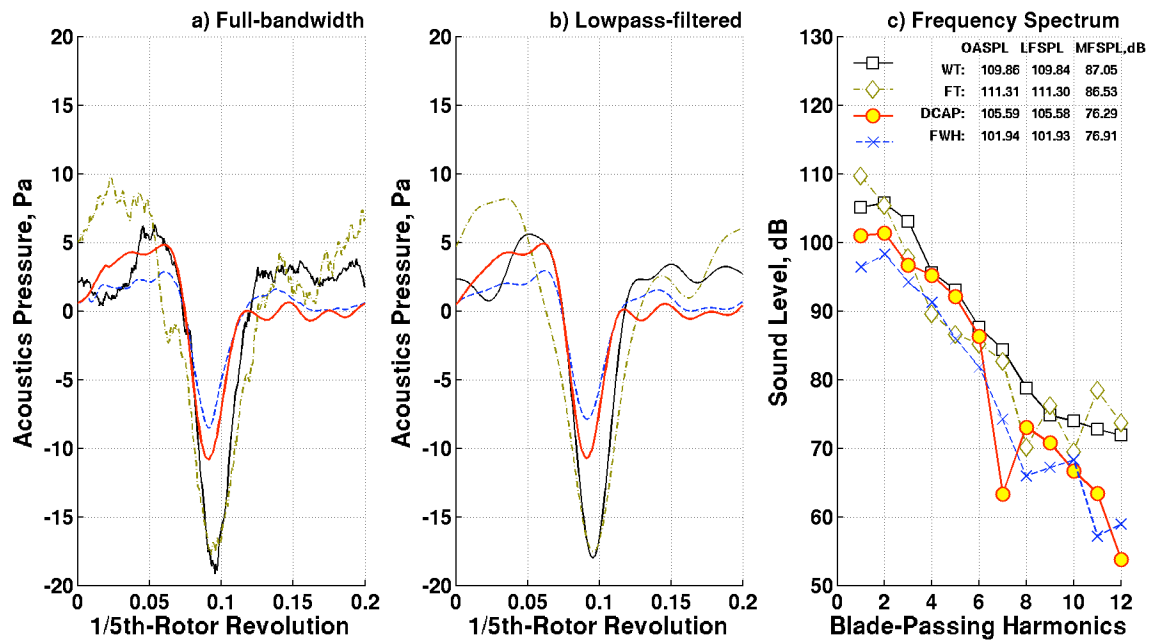
Figure 11 (continued). Predicted acoustic time histories for the different advance ratios at microphone M13.

The corresponding acoustic time histories, at microphone M13, for the four advance ratio conditions are illustrated in Figure 11. For the lower advance ratio conditions (μ = 0.165 and 0.200), DCAP predictions are unable to account for the high frequency, impulsive noise fluctuations due to constraints imposed by the grid spacing and finite-difference scheme. Large differences in the mid-frequency MFSPL metric, up to 20 dB, are observed between DCAP predictions and wind tunnel measurements.

Low frequency noise content are better captured by the direct CFD method. As shown in Figure 11b, the lowpass-filtered signals (< 200 Hz) from DCAP are in reasonable agreement compared to wind tunnel measurements. Overall, the DCAP results under-predicts the low frequency LFSPL metric by approximately 0.5 to 4.0 dB. These results demonstrate that the direct CFD method is not only capable of capturing thickness noise at higher advance ratios, but steady loading (in-plane) noise that dominants at lower advance ratios as well.

In contrast, the acoustic analogy-based predictions (FWH) appear to fair better for capturing high frequency noise contents. Impulsive noise fluctuations are predicted for the two lower advance ratio conditions with peak-to-peak amplitudes that are quite similar to wind tunnel measurements, albeit at different instances in time (blade azimuth). Low frequency noise contents are also well predicted at lower advance ratio conditions where steady loading noise mechanism dominates. At higher advance ratios, the acoustic analogy-based predictions become less accurate with upwards of 8.0 dB differences in LFSPL at μ = 0.300. Increased discrepancies in the LFSPL metric with advance ratios suggest that it may be due to the negligence of the flow-field effects off the blade tip near the advancing side of the rotor.

CONCLUSIONS

The use of CFD to directly predict helicopter main rotor source noise is shown to be quite promising as an alternative mean for low frequency noise evaluation. Results using existing state-of-the-art grid structures and finite-difference schemes demonstrated that small perturbation pressures, associated with acoustics radiation, can be extracted with some degree of fidelity.

Assessment of the direct CFD method is performed via comparing predicted results to conventional acoustic analogy-based predictions and with measurements from wind tunnel and flight test data. Evaluation of in-plane noise radiation of the MD-902 main rotor at several advance ratio conditions yields the following results:

- Low frequency noise contents, below 6th blade-passing harmonics, are reasonably well-captured using the direct CFD method with a grid spacing of about 12 inches at the microphone. Results are in general agreements with wind tunnel and flight test data to within 4 dB.

- Mid-to-high frequency noise contents cannot be predicted by the direct CFD method due to grid spacing constraints. Large discrepancies of up to 20 dB, in the mid-frequencies, are found especially at conditions dominated by impulsive noise fluctuations associated with blade-vortex interactions.

- Conventional "on-surface" acoustic analogy approach is better at predicting the overall noise at lower advance ratios where loading noise and impulsive noise dominate. At higher advance ratios where thickness noise becomes more important, low frequency noise tends to be under-predicted. It is speculated that this discrepancy is due to the flow-field effects off the blade tips not accounted for in the "on-surface" modeling.

REFERENCES

1. Potsdam, M. et. al., "Rotor Airloads Prediction Using Loose Aerodynamic/Structural Coupling," *Journal of Aircraft,* Vol. 43, No. 3, May-June 2006, pp. 732-742.

2. Ananthan, S. and Baeder, J. D., "Prediction and Validation of Loads on Bearingless Rotors Using a Coupled CFD-CSD Methodology," American Helicopter Society 64th Annual Forum & Technology Display, Baltimore, Montreal, Canada, April 29 – May 1, 2008.

3. Duque, E.P.N, Sankar, L.N, Menon, S., Bauchau, O., Ruffin, S., Smith, M., Ahuja, A., Brentner, K.S., Long, L.N., Morris, P.J., and Gandhi, F., "Revolutionary Physics-Based Design Tools for Quiet Helicopters" 44th AIAA Aerospace Sciences Meeting and Exhibit, Reno, NV January 2006, AIAA 2006-1068

4. Boyd, D. D., "HART-II Acoustic Predictions using a Coupled CFD/CSD Analysis," American Helicopter Society 65th Annual National Forum, Grapevine, TX, May 27-29, 2009.

5. Tam, C. K. W., "Computational Aeroacoustics: Issues and Methods," *AIAA Journal*, Vol. 33, No. 10., October 1995, pp. 1788-1796.

6. Colonius, T., Lele, S. K., "Computational Aeroacoustics: Progress on Nonlinear Problems of Sound Generation," *Progress in Aerospace Sciences*, Vol. 40, 2004, pp. 345-416.

7. Wells, V. L. and Renaut, R. A., "Computing Aerodynamically Generated Noise," *Annu. Rev. Fluid Mech.*, Vol. 29, 1997, pp. 161-199.

8. Baeder, J. D., "Euler Solutions to Nonlinear Acoustics of Non-Lifting Hovering Rotor Blades," NASA TM-103837, February 1991.

9. Nichols, R. H., Buning, P. G., "User's Manual for OVERFLOW 2.1," University of Alabama and NASA Langley Research Center, 2008.

10. Strawn, R., Nygaard, T., Bhagwat, M., Dimanlig, A., Saberi, H., Ormiston, R., and Potsdam, M., "Integrated Computational Fluid and Structural Dynamics Analyses for Comprehensive Rotorcraft Analysis," AIAA Paper 2007-6575, AIAA Atmospheric Flight Mechanics Conf., Hilton Head, SC, August 2007.

11. Johnson, W., "Technology Drivers in the Development of CAMRAD II," American Helicopter Society Aero-mechanics Specialists' Conference, San Francisco, CA, January 1994.

12. Wissink, A. M. Sitaraman, J., Sankaran, V., Mavriplis, D. J. Pulliam, T. H., "A multi-code python-based infrastructure for overset CFD with adaptive cartesian grids," AIAA Paper 2008-927, 2008.

13. Shirey, J. S., Brentner, K. S., Chen, H.-N., "A Validation Study of the PSU-WOPWOP Rotor Noise Prediction System," 45th AIAA Aerospace Sciences Meeting and Exhibit, Reno, Nevada, January 8-11, 2007.

14. M. J. Lighthill, "On Sound Generated Aerodynamically. I. General Theory," *Proc. R. Soc. Lond. A* **211** (1952) pp. 564-587.

15. Ffowcs Williams, J. E., and Hawkings, D. L., "Sound Generated by Turbulence and Surfaces in Arbitrary Motion", *Philosophical Transactions of the Royal Society*, Vol. A264, 1969, pp. 321-342

16. Farassat, F. and Succi, G. P., "The Prediction of Helicopter Rotor Discrete Frequency Noise," *Vertica*, Vol. 7, No. 4, pp. 309-320, 1983.

17. Straub, F. K., Anand, V. R., Birchette, T., Lau, B. H., "Wind Tunnel Test of the SMART Active Flap Rotor," American Helicopter Society 65th Annual Forum and Technology Display, Grapevine, TX, May 27—29, 2009.

18. Barbely, N. L., Sim, B. W., Kitaplioglu, C. K. and Goulding II, P., "A Study of Acoustic Reflections in Full-Scale Rotor Low Frequency Noise Measurements Acquired in Wind Tunnels," American Helicopter Society Aero-mechanics Specialists' Conference, San Francisco, CA, January 20-22, 2010.

19. Watts, M. E., Conner, D. A. and Smith, C. D., "Joint Eglin Acoustic Week III Data Report," NASA TM-2010-216206, March 2010.